White Rose
university consortium
Universities of Leeds, Sheffield & York

eprints@whiterose.ac.uk
https://eprints.whiterose.ac.uk/

Metal-shell nanocapsules for the delivery of cancer drugs

James Hitchcock△, Alison L. White§, Nicole Hondow△, Thomas A. Hughes†, Hanae Dupont‡, Simon Biggs⊥, Olivier J. Cayre△

△ School of Chemical and Process Engineering, University of Leeds, Leeds LS2 9JT, U.K.

§ Australian Institute for Bioengineering and Nanotechnology, University of Queensland, St Lucia, Queensland 4072, Australia

⊥The University of Western Australia, Perth, WA 6009, Australia

† School of Medicine, University of Leeds, St. James's University Hospital, Leeds LS9 7TF, U.K.

‡ Paul Pascal Research Centre, University of Bordeaux, Avenue du Dr Albert Schweitzer, 33600 Pessac, France

Cytotoxic drugs tend to have substantial side effects on healthy tissues leading to systemic toxicity, limited tolerated doses and reduced drug efficacy. A prominent research area focuses on encapsulating cytotoxic drugs for targeted delivery to cancer tissues. However, existing carriers suffer from low drug loading levels and high drug leaching high both when circulating systemically and when accumulating in non-target organs. These challenges mean that the few approved encapsulation technologies have not been widely adopted for clinical use. Recently, we have demonstrated efficient manufacture of impermeable metal-shell/liquid core microcapsules that permit localised delivery by triggering release with ultrasound. This method has the potential to improve on existing methods for localised drug delivery because it:

- Encapsulates high concentrations of low molecular weight hydrophobic drugs;
- Preventing leaching in non-target areas resulting in the possibility of drastically amplifying the enhanced permeability and retention (EPR) effect;
- Allows triggered release via ultrasound to deliver high drug doses locally

We demonstrate here the further miniaturization of both the emulsion droplet template and the thickness of the surrounding metal shell to the nanoscale in an attempt to take advantage of the EPR effect and allow for the excretion of the nanoparticles by the hepatobiliary system.

1.1 Introduction

The design and fabrication of nanoscale drug delivery systems (nanocarriers) to allow controllable encapsulation and release of therapeutic agents within the body has received a great deal of interest in the literature.[1-11] A particularly prominent research area focuses on the encapsulation of small cytotoxic drugs for intravenous delivery to cancer tissues.[12-14] Targeted encapsulation can allow for more efficient delivery to tumours than that achieved when the free drug is circulated systemically, thereby reducing off-target side-effects with potential increased efficacy. Consequently, encapsulation also has the potential of locally delivering higher drug concentrations for the same initial dose.

Numerous technologies have been proposed academically to achieve safer/more efficient chemotherapeutic drug delivery. Many rely on particulate-based drug carriers, which often take advantage of the EPR effect, a form of passive targeting, to allow the nanocarrier to preferentially accumulate at the tumour site. However, these carriers typically only achieve small improvements in efficacy as compared to systemic drivery of the free drug, often because drug leaching, particulary into non-targeted organs such as the liver, kidney and spleen,[12] is not prevented and therefore systemic toxicity is not averted,[9] particularly on dilution into the blood stream.[12] These drawbacks, in conjunction with the relatively weak EPR effect have, in part, contributed to very few nanocarriers being approved for transition to clinical practice.[13, 14]

In the last 15 years or so, localised triggered delivery methods[15-20] in combination with improved nanocarriers[10, 12] showing more efficient drug retention have offered hope of increasing drug dosage locally while reducing systemic side effects. Several triggering methods have been proposed to actively release drugs at the site of the tumours, in particular photothermal[15] or acoustic[19] methods, which enable remote activation of the drug carriers to release their cargo locally[16-20]. More recently, drug carriers where metal films/shells are used to provide a low permeability barrier show great promise in improving drug retention before release is activated. Indeed, such systems typically take advantage of the very low diffusion of drug molecules through the metal but also rely on their structural properties to allow induced fracture and consequently trigger the drug release. Sun *et al.* showed activated release from metal capsules using an ultrasonic probe however the colloidosome template based metal shell growth technique currently limits capsules to the micron size range.[21] Wang *et al* were able to synthesis metal nanocapsules based on polymeric vesicle templates and used near infra-red light to induce capsule rupture.[9] Although direct evidence of

leakage free nanocapsules was not demonstrated, in-vivo mouse work was evidenced.
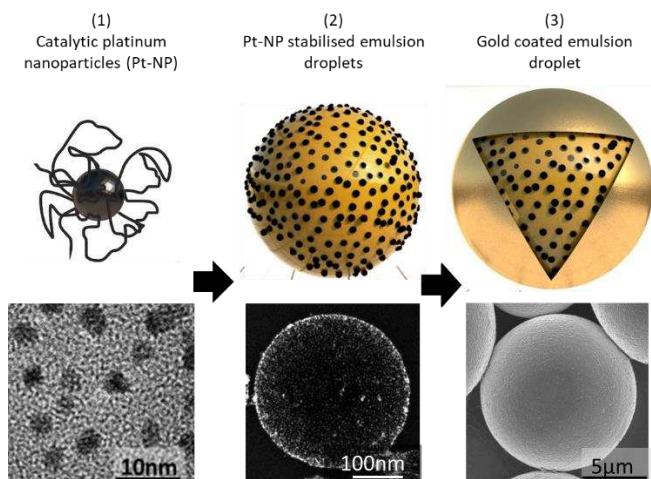

Figure 1. Schematic diagrams and examples of corresponding electron micrographs of the three synthesis steps leading to the preparation of metal capsules: (1) catalytic platinum nanoparticles (Pt-NPs) stabilised by a long chain polymer are first synthesised (2) the nanoparticles are then used to stabilise liquid emulsion droplets containing the dissolved drug to be encapsulated (a nanodroplet here was chosen to exemplify the surface position of individual PtNPs) and (3) an electroless deposition process is carried out to deposit a continuous, impermeable metal coating on the emulsion droplet to fully encapsulate the droplet core containing the drug.

Metal-shell nanocapsules could significantly improve existing delivery mechanisms as they have the potential for indefinitely retaining high doses of chemotherapy drugs, restricting systemic drug leaching[9] in other tissues known to accumulate nanoparticles[12] whilst allowing for safe build-up of drugs in tumours through the EPR effect before releasing high drug doses controllably using triggered release. This unique release profile coupled with extended capsule/carrier residency times (100 nm gold particle clearance times are more than 6 months[22-24]) could potentially provide an opportunity to amplify the weak EPR effect, extending drug delivery efficacy far beyond existing carriers.[25]

In addition metal nanocapsules are good ultrasound contrast agents[16, 25-27], which could also allow for image guided theranostics, important for ascertaining nanocapsule position and concentration prior to capsule rupturing using focused ultrasound. They also show low biological toxicity[23, 28] and are easily surface functionalised.[29] Previously demonstrated phased metal shell fracture[30] could also potentially allow for the administration of a single dose followed by multiple phased release of drug.

Recently, we have demonstrated the efficient manufacture of impermeable metal-shell/liquid core microcapsules[31] (Figure 1) that allow localised high dose delivery of small molecular actives by remotely triggering release with ultrasound at the target location.[30, 32] In this work, we use a metal film deposition process, where first platinum nanoparticles (Pt-NPs) are used to stabilise emulsion droplets, thus creating micron sized oil droplets with a dense packing of nanoparticles on their surface. Secondly, the adsorbed

nanoparticles are used as catalysts/nucleation sites at the oil-water interface for the electroless deposition of a continuous secondary metal film on the surface of the oil droplets. Previously, the resulting metal-shell microcapsules prepared with this method have been limited to a size range of approximately 500 nm to 20 μm, which although potentially appropriate for implantation in resection cavities, is not appropriate for systemic drug delivery.

This article translates the previous work described above towards much smaller impermeable metal-shell nanocapsules. Here we explore the possibility of reliably producing a Pt-NP stabilised nanoemulsion template with high particle density at the oil-water interface for use as a template for secondary metal film growth. The production of metal capsules from these nanoemulsion droplet precursors is then explored. Finally, we investigate the retention of a small model molecule within the capsules.

1.2 Materials and methods

Materials

The following chemicals were used as received: polyvinyl pyrrolidone (PVP, 40kDa, Fluka Analytical, >99%), Sodium tetrahydridoborate (NaBH$_4$, Sigma Aldrich, ≥98.0%), chloroplatinic acid hydrate (H2PtCl6-6 H2O, Sigma Aldrich, ≥99.9% trace metals basis), gold (III) chloride tetrahydrate (HAuCl4·3H2O, Sigma Aldrich, 99.99% trace metals basis), hexadecane (Sigma Aldrich, 99%), sunflower oil (Sigma Aldrich 99.99%), hydrogen peroxide (Sigma Aldrich H$_2$O$_2$, 30.5 wt%) and Paclitaxel (Taxus brevifolia, Fluorochem). Milli-Q water (18.2 MΩ.cm resistivity at 25°C) was obtained from a Millipore unit and used throughout all experiments.

Platinum nanoparticle synthesis

Pt-NPs were synthesised by the reduction of platinum salt in the presence of a reducing agent, Sodium tetrahydridoborate, at room temperature. H$_2$PtCl$_6$.6H$_2$O (0.23 g, 4.4 mM) was dissolved in a 0.0067 wt% PVP solution (100 mL). Under vigorous stirring, NaBH$_4$ (2 mL (1.2 M) was rapidly added into the mixture which was accompanied by a rapid change in colour from yellow to black. After stirring at 750 rpm for 2 minutes the nanoparticle suspension was filtered through a 0.2 μm pore size syringe filter, in order to remove any larger contaminates, and stored at 4 °C.

Gold film growth on platinum nanoparticles in suspension

To test the possibility of controlling the electroless deposition of very thin secondary metal films onto the Pt NPs, different gold film thicknesses were deposited on the surface of Pt-NPs when suspended in an aqueous continuous phase. This was achieved through the following method: 0.05 mL of the undiluted Pt-NP dispersion (synthesis described above) was added to Milli-Q water (10 mL). 1 mL of a PVP solution (40 KDa 0.05 wt%) and 0.025 – 1 mL of a 12 mM gold salt solution (HAuCl4) were added successively. The volume of gold salt added to the suspension was varied depending on the

desired final core/shell nanoparticle diameter. Finally, 1 mL of H_2O_2 (60 mM) was added to initiate the electroless deposition process and the vial was gently mixed by hand for 30 seconds.

Emulsification

Hexadecane (volumes ranging from 0.01 - 0.4 mL) was added to the Pt-NP dispersion (5 mL) and immediately pre-emulsified by vigorously shaking the sample by hand for approximately 5 seconds. The pre-emulsion was then homogenised using a Sonic Dismembrator Ultrasonic Processor (Model FB-505 Fisher Scientific) for 1 minute at 20% amplitude. A water bath at ambient temperature, (~20°C), was used to limit temperature increase of the emulsion during homogenisation whilst not causing the hexadecane to freeze (hexadecane melting point is 18°C). The resulting emulsions were then agitated on a carousel for 3 minutes and used subsequently without further processing.

In order to produce emulsions containing Paclitaxel, excess Paclitaxel was left to dissolve in sunflower oil for 24 hours and then filtered to remove undissolved drug (Giving a final solution concentration of ~13 mg.mL^{-1}). The emulsification step was then carried out using 0.4 mL of oil in the same way as described above for the hexadecane core Pickering emulsions.

Electroless deposition of metal shell

For both the hexadecane and the Paclitaxel in sunflower oil Pt-NP stabilised micron sized Pickering emulsions, 0.2 mL of undiluted Pickering emulsion was added to the following gold plating solution; 1 mL PVP solution (0.2wt%), 10mL of Milli-Q water, 2 mL of 12 mM gold salt ($HAuCl_4$) and 1 mL of H_2O_2 (60 mM). The samples were then agitated on the carousel for 30 minutes. Capsules were then allowed to settle under gravity for 24 hours and were subsequently washed by removal and replacement of the supernatant with Milli-Q water.

The nano-sized Pickering emulsions were metal coated by adding 0.05 mL of a homogeneously mixed Pickering emulsion (made with 0.01 mL of hexadecane) to the same plating solution as described above apart from the volume of the gold salt solution (12 mM), which was varied from 0.025 to 2 mL depending on the desired film thickness. In order to keep the plating volume the same, samples using a lower volume of gold salt were topped up to the constant total volume used throughout these procedures with Milli-Q water.

Characterisation

Optical microscopy: Microcapsules were observed using an Olympus BX51 optical microscope.

Emulsion size distribution measurements: For sub-micron emulsion droplets, a NanoSeries Zetasiser (Malvern Nano-ZS) (DLS) fitted with a He-Ne laser source (633 nm wavelength, 4 mW power) was used to measure droplet size distribution. For emulsion droplets larger than 1 μm, droplet size distribution was measured using a Benchtop C70 Series FlowCAM imaging flow cytometry instrument used in AutoImage mode with a 20x objective, FC50 flow cell in a reverse flow configuration to ensure that all droplets are passed through the measurement cell.

Scanning electron microscopy (SEM): a LEO 1530 Gemini field emission gun scanning electron microscopy (FEGSEM) was used to image metal-shell microcapsules. No conductive coating is applied for these observations.

Transmission electron microscopy (TEM and CryoTEM): Nanoparticle samples were analysed using a FEI Tecnai TF20 field emission transmission gun electron microscope (FEGTEM) fitted with a HAADF detector and GatanOrius SC600A CCD camera. An Oxford Instruments INCA 350 EDX system/80 mm X-Max SDD detector was used for elemental mapping. Prior to analysis, samples were deposited on a TEM grid (holey carbon film, 400 Cu Mesh from Agar Scientific) and allowed to dry. It should be noted that this method only takes account of the metallic nanoparticle cores and not the PVP polymer 'shell', an example of one such image can be found in figure 8. Particle sizes where then determined using ImageJ software using the following method: TEM images were first adjusted for contrast, the threshold size was then set to a surface area 2−28 nm^2, and the circularity was set to 0.2−1.00. The resulting image was then made binary and the particle diameters were automatically analysed to give a size distribution for the suspension.

Nano-sized Pickering emulsion droplets were imaged using an FEI Titan3 Themis G2 Cryo-TEM operating at 300kV fitted with 4 EDX silicon drift detectors and a Gatan One-View CCD. For cryo-EDX spectroscopy, Bruker Esprit v1.9 software was used along with probe currents between 40 and 100 pA and a dwell time of 23 μs. High angle annular dark field scanning transmission electron scanning mode was used (HAADF STEM). 0.1 mL of suspension was allowed to flow through a lacey carbon coated TEM grid (EM Resolutions) onto a blotting tissue underneath the grid. Samples were then immediately (to avoid complete drying of the sample) blotted (blot force 6) and plunged into liquid ethane. A Gatan 914 cryo-holder was used and the temperature was maintained below -160°C to prevent devitrification.

The same Cryo-TEM procedure was used to measure Pt-NP densities at Pickering emulsion droplet interfaces. Pickering emulsion droplets were made binary in colour, manually using ArtStudio (5.103). The binary images were then analysed for surface area coverage using ImageJ software and apparent nanoparticle surface densities were corrected for emulsion drop curvature. Both methods are described in a previous publication.[33]

Hexadecane core retention testing using gas chromatrapy (GC)

100% of the gold coated capsule dispersion was allowed to settle under gravity for 48 hours (Settling rates increase dramatically between the nano-Pickering emulsions and the corresponding thickest (15-20 nm) gold shell nanocapsules due to a combination of both a significant increase in mean density due to the gold (19.3 gcm^3) and increased diameter). The water above the capsules was removed and the sample was replenished with Milli-Q water to reach a total volume of 2 mL. 8 mL of absolute ethanol was then added to yield a capsule suspension in a 4:1 ethanol:water continuous phase. The capsules were periodically gently stirred and 1.5 mL samples was taken and centrifuged at 7000 rpm for 1 minute (Eppendorf Minispin) to remove the capsules by sedimentation. The supernatant was analysed with a Perkin Elmer Clarus 580GC using the following method and column: Elite-1 capillary column, length 30 m, internal diameter 0.25 mm. The column temperature was programmed from 50°C to 300°C at 20°C/min at a flow rate of 2 mL/min.

Paclitaxel retention testing using high pressure liquid chromatography–mass spectrometry and UV detector (HPLC-MS-UV)

Release of paclitaxel from microcapsules was measured as follows. Firstly, all of the gold coated microcapsules were allowed to settle under gravity for 2 hours (sedimentation rates of the capsules were calculated – see figure 6 and equation 1 - in order to confirm this time was sufficient). The water above the capsules was removed and the suspension was replenished with Milli-Q water for a total volume of 2 mL. The maximum solubility of paclitaxel in the discarded aqueous supernatant is negligible meaning that the potential effect of losses incurred in the aqueous phase on the measurement process is also negligible. 8 mL of acetonitrile was then added to obtain a suspension in a 4:1 ratio of acetonitrile to water.

The capsules were then periodically, gently stirred and 1.5 mL samples were taken and centrifuged at 7000 rpm for 1 minute (Eppendorf Minispin) to remove the capsules by sedimentation. The supernatant was then analysed using HPLC. Release from the control, uncoated Pickering emulsion, against which the previous samples were normalized, was tested as follows. 0.2 mL of the re-dispersed Pickering emulsion was added to 1.8 mL of Milli-Q water and 8 mL of acetonitrile. The vial was then periodically, gently stirred and 1 mL samples were taken and centrifuged at 7000 rpm for 1 minute to remove any platinum nanoparticles by sedimentation. It should be noted that on dissolution of the Sunflower oil core from the Pickering emulsions, the platinum nanoparticle stabilising 'sheets' aggregate in the acetonitrile and therefore sediment well under the centrifugal conditions described above. The supernatant was then analysed by HPLC. For both samples, the mobile phase was acetonitrile/water, with a gradient of 5-90 % acetonitrile over 5 minutes and a flow rate of 0.5 mL/min. The column used was an Ascentis Express C18, 50 x 2.1 mm with a 2.7 µm

particle size. UV detection was measured at 230 nm wavelength.

1.3   Results and discussion

The work presented in this article builds on our previous studies that demonstrated control of metal-shell microcapsule physical properties such as size, shell thickness and core type.[30-32] In addition, our recent work demonstrated direct growth of a gold film on the surface of emulsion droplets stabilised by nanoparticles which act as a nucleation site for an electroless deposition process. Remotely triggering metal shell fracture using ultrasound was also shown to be achievable to activate core release.[30] Here, we further demonstrate (i) encapsulation of a cytotoxic drug in such metal-shell microcapsules and (ii) development of metal-shell nanocapsules with sizes suitable for (leaching-free) systemic delivery. Thus, we first aim to confirm that metal-shell microcapsules, of mean diameter ~10 µm and shell thickness ~50 nm, are able to permanently encapsulate Paclitaxel, a typical chemotherapy drug of the taxane family, which is used in treatment of many common cancers including breast cancer. For this purpose, we emulsified 0.4 mL of sunflower oil containing Paclitaxel at a concentration of ~13 mg.mL^{-1} with 5mL of a Pt-NP aqueous dispersion. The resulting oil/water Pickering emulsion droplets were metal coated and tested for release/leaching of the drug in an acetonitrile/water continuous phase chosen to enable complete dissolution of the encapsulated drug if leaching occurs (see method section for full description). We then monitored the percentage of Paclitaxel remaining encapsulated over time (Figure 2).
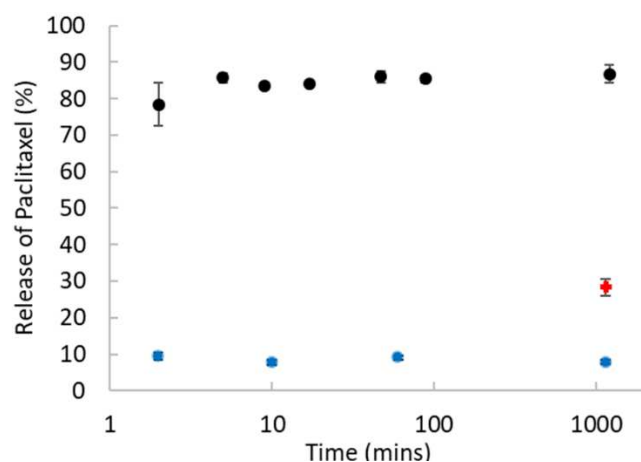

Figure 2: Drug release monitored over time via HPLC for (●) the uncoated Pickering emulsion used as a permeable carrier control and for (●) metal-shell microcapsules into a phase in which the core readily dissolves (80% acetonitrile, 20% water). (✚) - represents the subsequent paclitaxel release activated with an ultrasonic probe.

Figure 2 confirms that Paclitaxel in a sunflower oil carrier can be encapsulated, in a metal shell, without leaching in an acetonitrile continuous phase, which readily dissolves both core species. The capsules were able to retain, without leakage, ~90% of the core phase over at least 16 hours. The subsequent core release method using mechanical fracture via ultrasonic probe (see methods for details) does not recover all of the encapsulated Paclitaxel. This is likely for two reasons:

a) A proportion of the capsules remain unbroken; and, b) Paclitaxel adsorbs onto metal capsule fragments, which are removed during the centrifugation before characterising the concentration of drug present in the sample continuous phase.

Production of nanoscale Pickering emulsions

In order to produce liquid core metal capsules, which can be used as intravenous drug delivery vehicles, able to take advantage of the EPR effect and be excreted by the biliary system, the metal-shell capsules need to be approximately 100 nm in diameter.[34, 35] As a result, the size of the initial emulsion droplet templates needs to be reduced to such dimensions, while retaining a high particle density at the oil-water interface. We therefore used the same optimised Pt-NP dispersion in order to avoid competitive interfacial adsorption of excess PVP polymer during emulsification.[33] We then used ultrasonic probe homogenisation and manipulated the emulsion oil-to-water ratio in order to reduce the resulting oil droplet size.

Figure 3 shows the obtained Pickering emulsions, 10 hours after emulsification, when hexadecane, used here again as a model oil, was homogenised with the Pt-NP aqueous dispersion using different oil/water ratios. All samples were homogenised with an ultrasonic probe for 1 min at 20% power amplitude. As demonstrated in a previous publication for larger droplets,[30] reducing the oil volume fraction in these emulsions leads to a decrease in droplet diameter, which is here manifested by both a change in the droplet creaming rate (Figure 3) and in the droplet sizes (Figure 4). Here, the droplet total surface area remains approximately constant independently of the oil volume fraction (Figure 5) and thus the droplets increase in size as the oil volume fraction is increased. This is a result of (almost) all the nanoparticles adsorbing at the oil/water interface to stabilise the emulsion (as demonstrated by the high light transmittance of the creamed emulsion continuous phase) and a process of limited coalescence driving full particle coverage at the interface. Both of these phenomena have been discussed previously.[30]
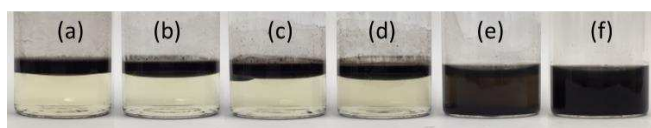

Figure 3: Digital photographs of Pt-NPs-stabilised emulsions for different oil volume ratios: a) 8 vol%, b) 4 vol%, c) 2 vol%, d) 1 vol%, e) 0.4 vol% and f) 0.2 vol%. All samples are shown 10 hours after preparation (1 min ultrasonic homogenisation at 20% amplitude). 5 mL of Pt-NP dispersion as the aqueous continuous phase was used in each case.

Figure 4 shows the resulting mean emulsion droplet sizes as a function of oil to continuous phase volume ratio. Droplets of diameter more than 1 μm were measured by optical microscopy by analysing a large number of images of the dispersion as it flows through a microfluidic channel (Flowcam). Droplets of diameters below 500 nm were measured by dynamic light scattering (DLS) (Zetasizer).
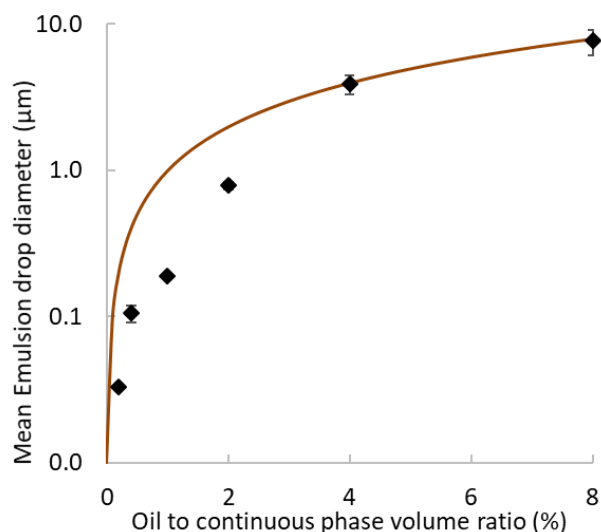

Figure 4: Mean emulsion droplet size as a function of oil/water (hexadecane / Pt-NP dispersion) phase ratio. The continuous line represents the theoretical droplet size as a function of total volume of oil in the sample calculated using the (constant) expected total surface area the Pt-NPs are able to cover which itself is based on CryoTEM imaging. 2D Pt-NP surface density was measured to be ~34% and is denoted as β in equation S3 in the supplementary information (see cryo-TEM methods section for the experimental description)

Figure 4 demonstrates that, by using an optimized Pt-NP dispersion[33] and altering the ratio of the dispersed phase (core oil) to the continuous phase (Pt-NPs aqueous dispersion), the mean size of the resulting emulsion droplets can be tuned from approximately 10 μm down to the 100 nm target diameter and below. The fitted line represents the theoretical droplet size as a function of oil volume present in the emulsions using the total surface area the Pt-NPs are able to cover as measured via cryo-TEM from the emulsion samples (NPs surface coverage was measured as ~34% and is denoted as β in equation S3 in the supplementary information). The improved fit at higher dispersed phase volume ratios is possibly due to some level of dispersed phase loss to the vial surface at the very low volumes (high oil/Pt-NP volume ratios).

To characterise further these emulsion droplets, two particular oil volume ratios were studied, namely 8% and 0.4%, for which large droplets above 1 μm and small droplets around 100 nm are formed, respectively. Optical microscopy was used to observe the larger droplets, which showed typical structures for this particular system (Figure 5a). However, for the smaller droplets, it was necessary to use Cryo-TEM to perform the same experiment, which consequently also allowed for the position and density of the Pt-NPs stabilisers to be identified (Figure 5b).
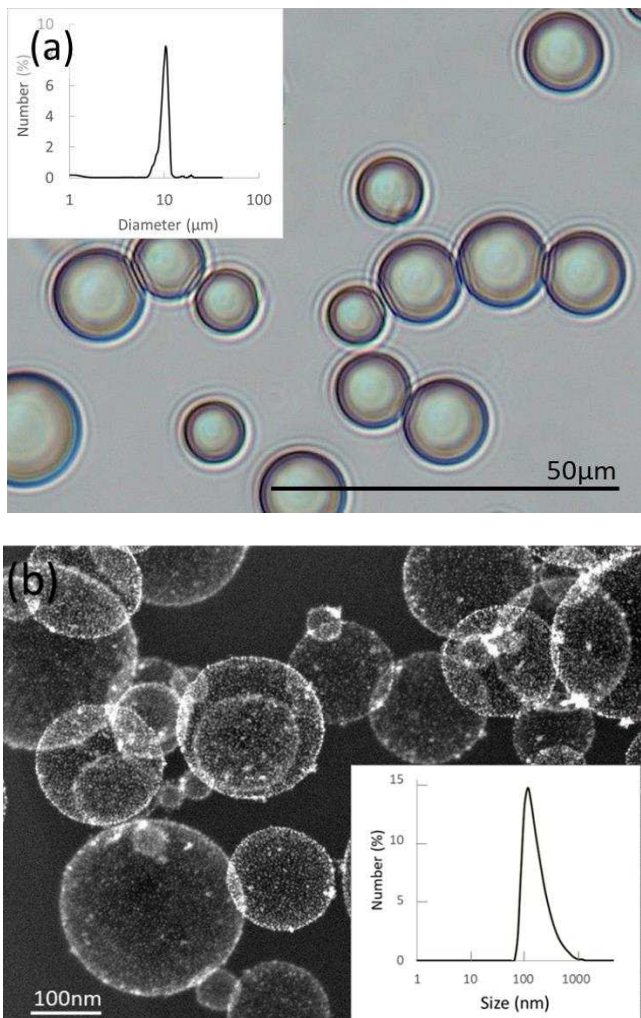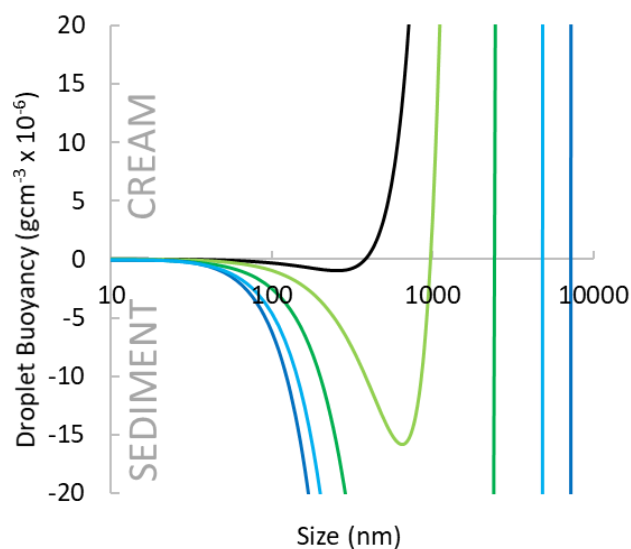
Figure 6: shows calculated buoyancy relative to water as a function of diameter for the primary Pickering emulsion (■) and metal capsules of various anticipated metal film thicknesses, 2 nm (■), 5 nm (■), 10 nm (■) and 15 nm (■).

From these data, it is clear that a minimum in buoyancy is observed for all systems as the large oil core volume dominates for high droplet/capsule sizes and the metal components of the surface (Pt-NPs and secondary gold shell) dominates for low droplet/capsules sizes. Thus, we expect that it is possible to separate the smallest Pickering emulsion droplets from droplets around 600 nm and above in these particular emulsion samples.

Equation 1 represents a version of Stokes law modified to be specifically applicable to a Pickering emulsion droplet travelling in a liquid under a centrifugal force (see supplementary information S1 for derivation). This equation was used to calculate settling time of the smallest droplets for a particular centrifugal speed in order to design an experiment where a broad size distribution can be split into the creaming and sedimenting populations.

$$t = \frac{18\mu ln\left(R_f/R_i\right)}{D_e^2\omega^2\left(\left(\frac{4\beta\rho_{np}D_{np}}{D_e} + \rho_{oil}\right) - \rho_f\right)}$$

Equation 1

Where: D_e Pickering emulsion drop diameter (m), β 2D fractional nanoparticle surface area coverage on the emulsion drop surface, D_{np} nanoparticle metal core diameter (m), μ fluid dynamic viscosity (Pa.s), R_f final radius of rotation (m), R_i initial radius of rotation (m), ρ_{np} nanoparticle metal core density (kg/m³), ρ_{oil} emulsion drop oil density (kg/m³), ρ_f continuous phase density (kg/m³), ω is the angular velocity (radian/s), t time to sediment from R_i to R_f (s).

Cryo-TEM was used in conjunction with particle counting software (imageJ) to measure the average Pt-NP core 2D

Figure 5: (a) Optical micrograph of Pt-NP stabilised Pickering emulsion droplets, the inset shows the size distribution (measured by Flowcam). Oil to continuous phase volume fraction was 8% and (b) shows a cryo-HAADF STEM micrograph of Pt-NP stabilised Pickering emulsion droplets of d50 ~100 nm , the inset shows the size distribution measured by dynamic light scattering. Oil to continuous phase volume ratio was 0.4%. In both cases the ultrasonic probe homogeniser was used to prepare the emulsions at a power of 20% for 1 min.

Nano-sized Pickering emulsion droplet size measurements showed a D50 of 108 nm, with a relatively broad size distribution highlighting the presence of some larger droplets, which were not suitable for the intended drug delivery purposes. As a consequence, the smaller emulsion droplets need to be isolated for further use. Thus, in the following sections, the 2D nanoparticle density is characterised with a view to primarily growing very thin impermeable secondary metal films but also assessing emulsion droplet buoyancy to explore the potential of purification by centrifugation.

Nano-Pickering emulsion buoyancy and 2D nanoparticle surface density

In addition to providing essential information used to tightly control secondary metal film growth, understanding 2D platinum nanoparticle density provides insight into the Pickering emulsion properties and subsequent metal-shell capsules settling behaviour. For a particular core, (hexadecane in this case), it is possible to use this information to isolate the smaller capsules within a suspension through size selection using centrifugation. Figure 6 shows calculated

densities on the surface of the Pickering emulsion droplets produced here and to verify that high Pt-NP densities are achieved. The mean Pt-NP core density was measured to be ~34% and was shown to be independent of Pickering emulsion drop size. High particle surface coverage is expected based on previously measured densities at liquid/solid interface.[33]·[36]

Figure 7a demonstrates the possibility of separating the Pickering emulsion droplets into two populations via centrifugation. The graph shows three size distributions for the original Pickering emulsion and the separated (creamed and sedimented) emulsion layers post centrifugation.
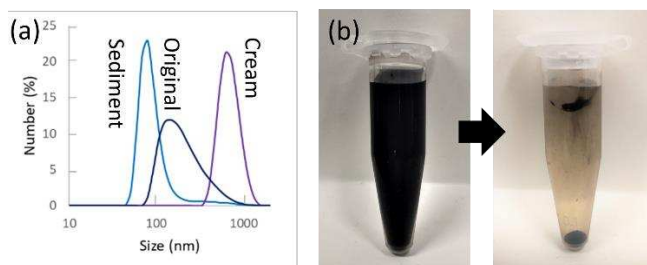

Figure 7a shows a graph of size distributions measured by DLS. The 3 size distributions represent the original Pickering emulsion and the creamed and sedimented layers post centrifugation, (b) are photographs of the Pickering emulsion pre and post centrifugation (note that the creamed layer appears lower than the liquid surface due to the angle at which the tubes were centrifuged)

As predicted from Figure 6, the Pickering emulsion droplets separated by size with larger droplets creaming and sub ~600 nm droplets sedimenting. Importantly, after centrifugation, it was possible to easily redisperse the small Pickering emulsion droplets (as seen in Figure 7a from the subsequent size distribution measurement) for deposition of the secondary gold films.

The system which allowed for the production of the smallest droplet sizes was thus chosen and used in the following section as a template for secondary metal film growth by electroless deposition.

Fine control over secondary metal film growth

In order to understand secondary metal film growth onto the Pickering 'nanoemulsion' droplets, we first tested the achievable control of secondary metal deposition on freely dispersed Pt-NPs (Fig. 8a to 8e). The mass of gold salt required to grow the Pt-NP 'seeds' from their original mean size of approximately 3 nm to larger diameters up to 6 nm was first calculated. Final particle sizes were specifically chosen to be approximately half the mean inter-nanoparticle spacing on the Pickering 'nanoemulsion' surface (~12 nm, measured by Cryo-TEM).

Subsequently, the Pickering 'nanoemulsion' droplets were used to understand and tightly control the early stage secondary film growth (Fig. 8f to 8j). This study was conducted with the long-term aim of reproducibly producing ultra-thin, continuous metal films onto such small droplets to

maximise the core content of the resulting 'nanocapsules'. The measured Pt-NP density at the droplet interface was again used here to assess the minimum mass of gold required to bridge the mean Pt-NP core inter-particle spacing (excluding the PVP stabilising layer) with the growing gold film, which allow for precisely tuning the gold salt concentration in the electroless deposition process. Thus, in targeting very thin gold films, we also use Cryo-TEM to characterise the early stage of the secondary metal film growth on the Pickering nano-sized emulsion droplet surface.

Figure 8 (a-j) show nanoparticle dispersions at the same concentration either as a free dispersion or on a Pickering nano-sized emulsion droplet surface. (a) shows the original Pt-NP and (b-e) show progressively larger platinum core, gold shell particles. (a* and d*) show TEM micrographs of the nanoparticles in (a) and (d) respectively. Figure 8(f-j) show the corresponding Pickering nano-sized emulsions.
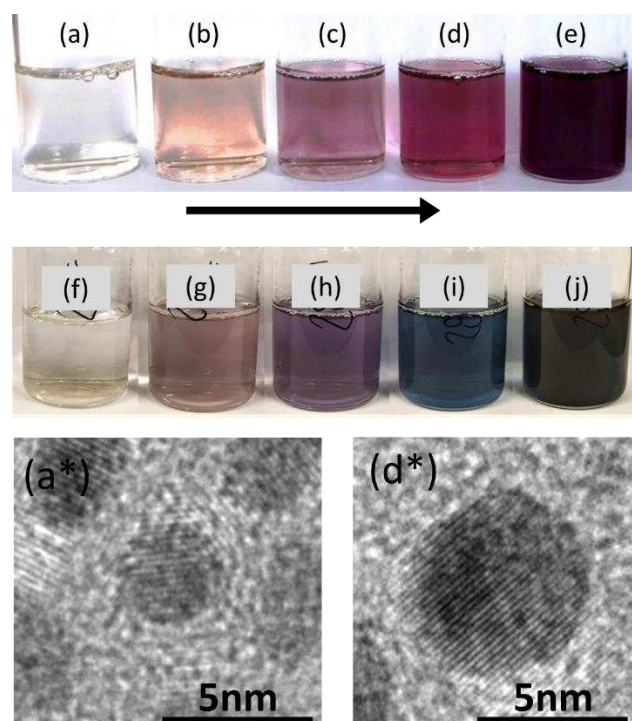

Figure 8 (a-j) show nanoparticle dispersions at the same concentration either as a free dispersion or on a Pickering emulsion droplet surface (200 times dilution of the original Pt-NP dispersion (see methods)). (a) shows the original Pt-NP and (b-e) show progressively larger platinum and gold core / shell particles. (a* and d*) show TEM micrographs of the nanoparticles in (a) and (d) respectively. (f- j) show the corresponding Pickering nano-sized emulsions.

It is interesting to note the shift towards the shorter wavelengths (Figure 8h-i). The colour change from red to blue which deviates from the colours of the series of free nanoparticle samples (Figure 8a-e) would appear to mark the onset of film formation as the growing nanoparticle Pickering emulsion 'sheet' becomes a full film. Thin sputter coated gold films have been shown to appear blue in transmitted light.[37]

Figure 9 shows a graph of nanoparticle diameter, as measured by TEM of the nanoparticles shown in Figure 8a-e, as a function of the mass of gold added. The red dot shows the

mean nanoparticle size measured by cryo-TEM on the equivalent Pickering nano-sized emulsion droplet interfaces.
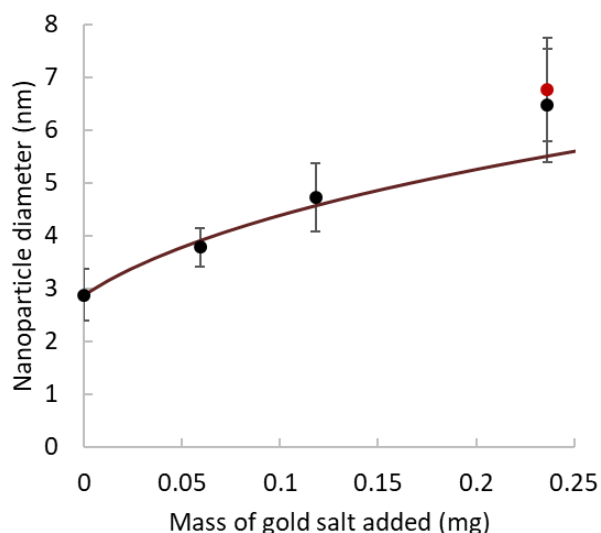
We can see from Figure 9 that the size of the nanoparticles associated with the Pickering nano-sized emulsion droplet surface fit well with those in the free dispersion. The continuous line represents a fit calculated from the mass of gold salt used to grow the underlying Pt-NP cores and the number and mean size of the Pt-NPs used (see equation S4 in the supplementary information). The under prediction of the fit at larger composite Pt core, Au shell nanoparticle diameters may be due to non-spherical deviation which was assumed in the calculations. Figure 10 shows the corresponding cryo-TEM micrographs of examples of both the original Pickering nano-sized emulsion interface and one where the nanoparticles have been grown to a mean diameter of 6 nm.
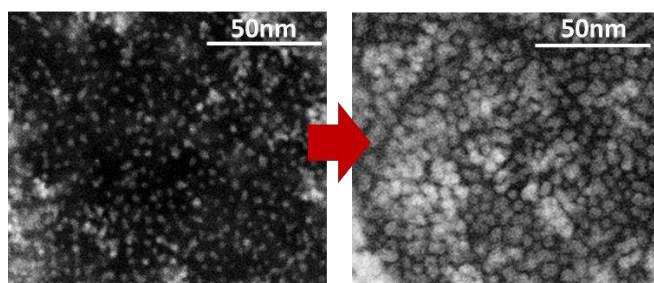

Figure 10 Cryo-TEM micrographs showing the Pt-NP spacing on nano-Pickering emulsion droplets before and after gold growth. Samples are taken from dispersions (a) and (d) pictured in Figure 11.

This provides exquisite control over the very early secondary film thickness (~3-6 nm) and allows for the production of films which are independent of both Picking nanno-sized emulsion size distribution and the number of excess Pt-NPs in the continuous phase (note that the emulsions used here are designed to form with little or no nanoparticles left over in the continuous phase and therefore we expect very few to be present, as evidenced by the low number of free nanoparticles visible in the amorphous water cryo-TEM image backgrounds (Figure 5b and Figure 11a)).

Figure 11 shows cryo-TEM images of a Pickering nano-sized emulsion drop with successively thicker gold films on their surfaces (Figure 11a-c). Although the images were chosen from polydisperse samples it should be notes that secondary gold film growth is independent from the underlaying droplet diameter and therefore any chosen capsules surface structure should be representative, (d) shows a wider field Cryo-TEM image of the sample (b) was chosen from.
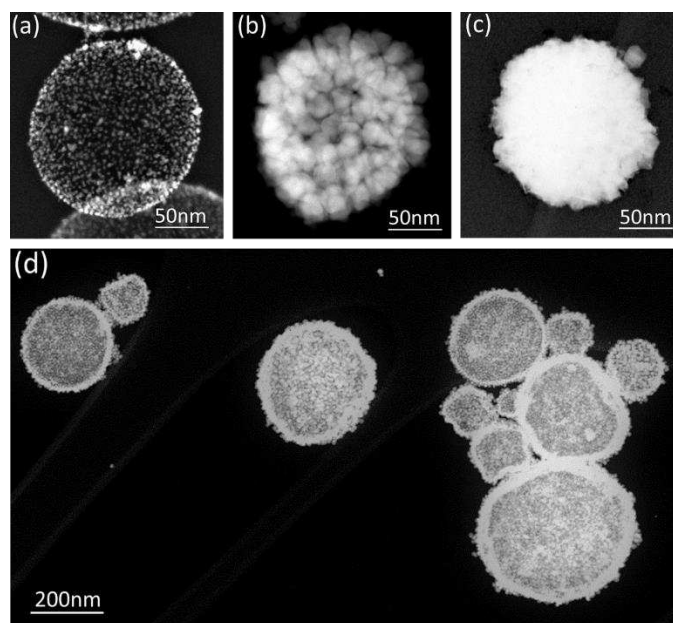

Figure 11 shows CryoTEM images of (a) a nanoPickering emulsion drop with (b and c) successively thicker gold films on its surface. Images were chosen from a more polydisperse samples, (d) shows a more representave wider field CryoTEM image of the sample (b) was chosen from.

Interestingly, as the distance between the growing nanoparticles on the Pickering nano-sized emulsion surface reduced, and they came into close proximity, the growth became somewhat inhomogeneous and therefore films needed to be grown thicker than the theoretical minimum (on the basis of the inter-nanoparticle spacing) in order to achieve complete coverage. This is likely due to Ostwald ripening occurring when the growing nanoparticle size differential becomes significant. These initial observations match reports from the literature that suggest metal nanoparticle seeded growth of homogeneous thin (less than 20 nm) complete metal films is difficult to achieve.[38-41] At close range, surface atoms are more readily able to migrate or even desorb and redeposit on a different surface[42] thus lowering local surface energies and therefore surface area volume ratios.

Nanocapsule core retention

Finally, we demonstrate that the resulting nanocapsules are able to retain a small model molecule in a continuous phase in which the core readily dissolves, a characteristic previously demosntrated for micron-sized capsules.[30-32]

Figure 12 introduces data for core release over time as measured by GC for both the uncoated Pickering nanoemulsion droplets and the metal coated nanocapsules.
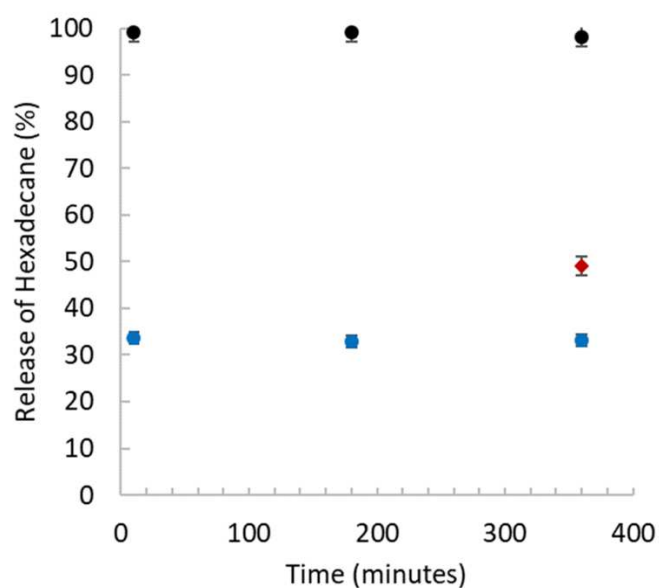

<u>**Figure 12**</u>: Hexadecane core release (molecular weight comparable to that of most cancer drugs – 226 g.mol^{-1}) into ethanol/water (4:1) for the nano Pickering emulsion droplets (●) and metal-nano nanocapsules (●). The last data point (◆) demonstrates release achieved from the metal nano-capsules when initiating metal film fracture using an ultrasonic probe.

The uncoated Pickering emulsion droplets released 100% of their core into the ethanol:water (4:1) continuous phase quickly as would be expected, given the very large surface to volume ratio, porosity of the Pt-NP film to hexadecane and the solubility of hexadecane in the continuous phase. For similar reasons, we would expect any incomplete metal shelled nanocapsule to release their core fully and quickly. The ~65% oil retention for 6 hours seen for the metal coated nanoemulsions shows that a large proportion of these nanocapsules achieve permanent encapsulation in this sample. An ultrasonic probe was then used to fracture and release the remaining oil. Through this process a further ~15% of the core hexadecane is released, demonstrating that oil has indeed been encapsulated efficiently within these metal-coated nanocapsules. Not all the core hexadecane is retrieved in these measurements, which indicates that only a proportion of the nanocapsule metal films are ruptured under these sonication conditions.

1.4   Conclusions

We demonstrate a method that adapts our previously developed production of metal microcapsules to achieve much smaller nano-sized capsules with the objective of creating impermeable capsules that can be circulated intravenously.

In this work, we firstly demonstrate that the size of the Pickering emulsion precursor can be controlled by limiting the total amount of interface created by the high-energy emulsification process through varying the oil to water ratio in the emulsion for a fixed number of nanoparticle stabilisers.

Subsequently, we develop a mathematical model to predict the separation of the nano-Pickering emulsion based on their size when centrifugation is used. This model is then verified experimentally, which leads to Pickering nano-sized emulsion precursors that can be used to prepare metal-shell capsules of appropriate dimensions for the intended application. In addition, by replicating gold shell growth on free Pt-NPs in suspension, we verify that the early stages of gold film growth on Pickering emulsion stabilized with the same Pt-NPs leads to films of equivalent thicknesses. However, it is clear that the proximity of the nanoparticles at the oil-water interface influences the early stage growth and more fundamental studies at these very short reaction times need to be carried out to understand how to obtain very thin, impermeable metal films via electroless deposition.

Nevertheless, our study demonstrates that a typical cancer drug molecule can be retained indefinitely within larger metal microcapsules and that a model small molecule can also be permanently retained and released using an ultrasonic probe from metal nanocapsules.

This work illustrates the potential of such metal nanocapsules for safely circulating highly potent drugs within the blood stream without undesired drug leaching prior to inducing localised release via ultrasounds.

1.5   References:

[1] D.H. Hu, P. Gong, Y.F. Ma, L.T. Cai, Research advancement and prospects of nanotechnology in early diagnosis and treatment of cancer, Chinese Journal of Cancer 28(9) (2009).
[2] J. Shi, Z. Xiao, N. Kamaly, O.C. Farokhzad, Self-assembled targeted nanoparticles: evolution of technologies and bench to bedside translation, Accounts of chemical research 44(10) (2011) 1123-1134.
[3] A.G. Cuenca, H. Jiang, S.N. Hochwald, M. Delano, W.G. Cance, S.R. Grobmyer, Emerging implications of nanotechnology on cancer diagnostics and therapeutics, Cancer 107(3) (2006) 459-466.
[4] G. Bao, S. Mitragotri, S. Tong, Multifunctional nanoparticles for drug delivery and molecular imaging, Annual review of biomedical engineering 15 (2013) 253-282.
[5] X. Wang, L. Yang, Z.G. Chen, D.M. Shin, Application of nanotechnology in cancer therapy and imaging, CA: a cancer journal for clinicians 58(2) (2008) 97-110.
[6] V. Sanna, M. Sechi, Nanoparticle therapeutics for prostate cancer treatment, Maturitas 73(1) (2012) 27-32.
[7] S.R. Grobmyer, D.L. Morse, B. Fletcher, L.G. Gutwein, P. Sharma, V. Krishna, S.C. Frost, B.M. Moudgil, S.C. Brown, The promise of nanotechnology for solving clinical problems in breast cancer, Journal of surgical oncology 103(4) (2011) 317-325.
[8] T. Bollhorst, K. Rezwan, M. Maas, Colloidal capsules: nano-and microcapsules with colloidal particle shells, Chemical Society Reviews 46(8) (2017) 2091-2126.
[9] L. Wang, Y. Yuan, S. Lin, J. Huang, J. Dai, Q. Jiang, D. Cheng, X. Shuai, Photothermo-chemotherapy of cancer employing drug leakage-free gold nanoshells, Biomaterials 78 (2016) 40-49.

[10] Y. Cao, F. Liu, Y. Chen, T. Yu, D. Lou, Y. Guo, P. Li, Z. Wang, H. Ran, Drug release from core-shell PVA/silk fibroin nanoparticles fabricated by one-step electrospraying, Scientific reports 7(1) (2017) 11913.

[11] Q. Sun, H. Gao, G.B. Sukhorukov, A.F. Routh, Silver-coated colloidosomes as carriers for an anticancer drug, ACS applied materials & interfaces 9(38) (2017) 32599-32606.

[12] A. Wicki, D. Witzigmann, V. Balasubramanian, J. Huwyler, Nanomedicine in cancer therapy: challenges, opportunities, and clinical applications, Journal of controlled release 200 (2015) 138-157.

[13] V.J. Venditto, F.C. Szoka Jr, Cancer nanomedicines: so many papers and so few drugs!, Advanced drug delivery reviews 65(1) (2013) 80-88.

[14] P.V. Devarajan, S. Jain, Targeted drug delivery: concepts and design, Springer2016.

[15] E. Boisselier, D. Astruc, Gold nanoparticles in nanomedicine: preparations, imaging, diagnostics, therapies and toxicity, Chemical society reviews 38(6) (2009) 1759-1782.

[16] P. Sontum, S. Kvåle, A.J. Healey, R. Skurtveit, R. Watanabe, M. Matsumura, J. Østensen, Acoustic Cluster Therapy (ACT)–a novel concept for ultrasound mediated, targeted drug delivery, International journal of pharmaceutics 495(2) (2015) 1019-1027.

[17] A. Van Wamel, P.C. Sontum, A. Healey, S. Kvåle, N. Bush, J. Bamber, C. de Lange Davies, Acoustic Cluster Therapy (ACT) enhances the therapeutic efficacy of paclitaxel and Abraxane® for treatment of human prostate adenocarcinoma in mice, Journal of Controlled Release 236 (2016) 15-21.

[18] J.M. Tsutsui, F. Xie, R.T. Porter, The use of microbubbles to target drug delivery, Cardiovascular Ultrasound 2(1) (2004) 23.

[19] O. Couture, J. Foley, N.F. Kassell, B. Larrat, J.-F. Aubry, Review of ultrasound mediated drug delivery for cancer treatment: updates from pre-clinical studies, Translational Cancer Research 3(5) (2014) 494-511.

[20] I. Udroiu, Ultrasonic drug delivery in Oncology, J BUON 20(2) (2015) 381-90.

[21] Q. Sun, Y. Du, E.A. Hall, D. Luo, G. Sukhorukov, A. Routh, A fabrication method of gold coated colloidosomes and their application as targeted drug carriers, Soft Matter 14(14) (2018) 2594-2603.

[22] E. Sadauskas, G. Danscher, M. Stoltenberg, U. Vogel, A. Larsen, H. Wallin, Protracted elimination of gold nanoparticles from mouse liver, Nanomedicine: Nanotechnology, Biology and Medicine 5(2) (2009) 162-169.

[23] S.C. Gad, K.L. Sharp, C. Montgomery, J.D. Payne, G.P. Goodrich, Evaluation of the toxicity of intravenous delivery of auroshell particles (gold–silica nanoshells), International journal of toxicology 31(6) (2012) 584-594.

[24] M. Longmire, P.L. Choyke, H. Kobayashi, Clearance properties of nano-sized particles and molecules as imaging agents: considerations and caveats, Future Medicine - Nanomedicine 3(5) (2008).

[25] S. Fokong, B. Theek, Z. Wu, P. Koczera, L. Appold, S. Jorge, U. Resch-Genger, M. van Zandvoort, G. Storm, F. Kiessling, Image-guided, targeted and triggered drug delivery to tumors using polymer-based microbubbles, Journal of controlled release 163(1) (2012) 75-81.

[26] J. McLaughlan, D. Cowell, S. Freear, Gold nanoparticle nucleated cavitation for enhanced high intensity focused ultrasound therapy, Physics in Medicine & Biology 63(1) (2017) 015004.

[27] O.K. Kosheleva, T.-C. Lai, N.G. Chen, M. Hsiao, C.-H. Chen, Selective killing of cancer cells by nanoparticle-assisted ultrasound, Journal of nanobiotechnology 14(1) (2016) 46.

[28] R.B. Weiss, R. Donehower, P. Wiernik, T. Ohnuma, R. Gralla, D. Trump, J. Baker Jr, D. Van Echo, D. Von Hoff, B. Leyland-Jones, Hypersensitivity reactions from taxol, Journal of Clinical Oncology 8(7) (1990) 1263-1268.

[29] P. Ghosh, G. Han, M. De, C.K. Kim, V.M. Rotello, Gold nanoparticles in delivery applications, Advanced drug delivery reviews 60(11) (2008) 1307-1315.

[30] K. Stark, J.P. Hitchcock, A. Fiaz, A.L. White, E. Baxter, S.R. Biggs, J. McLaughlan, S. Freear, O.J. Cayre, Encapsulation of emulsion droplets with metal shells for subsequent remote, triggered release, ACS applied materials & interfaces 11(13) (2019) 12272-12282.

[31] J.P. Hitchcock, A.L. Tasker, E.A. Baxter, S. Biggs, O.J. Cayre, Long-term retention of small, volatile molecular species within metallic microcapsules, ACS applied materials & interfaces 7(27) (2015) 14808-14815.

[32] A.L. White, C. Langton, M.-L. Wille, J. Hitchcock, O.J. Cayre, S. Biggs, I. Blakey, A.K. Whittaker, S. Rose, S. Puttick, Ultrasound-triggered release from metal shell microcapsules, Journal of colloid interface science 554 (2019) 444-452.

[33] J.P. Hitchcock, A.L. Tasker, K. Stark, A. Leeson, E.A. Baxter, S. Biggs, O.J. Cayre, Adsorption of catalytic nanoparticles onto polymer substrates for controlled deposition of microcapsule metal shells, Langmuir 34(4) (2018) 1473-1480.

[34] Y.C. Barenholz, Doxil®—the first FDA-approved nano-drug: lessons learned, Journal of controlled release 160(2) (2012) 117-134.

[35] R. Ngoune, A. Peters, D. von Elverfeldt, K. Winkler, G. Pütz, Accumulating nanoparticles by EPR: A route of no return, Journal of Controlled Release 238 (2016) 58-70.

[36] A. Toor, T. Feng, T.P. Russell, Self-assembly of nanomaterials at fluid interfaces, Eur. Phys. J. E 39(5) (2016) 57.

[37] T. Ung, L.M. Liz-Marzan, P. Mulvaney, Gold nanoparticle thin films, Colloids and Surfaces A: Physicochemical and Engineering Aspects 202(2-3) (2002) 119-126.

[38] M.A. Raza, H.J. Zandvliet, B. Poelsema, E.S. Kooij, Selective metallization by seeded growth on patterned gold nanoparticle arrays, Journal of applied physics 113(23) (2013) 233510.

[39] W. Ahn, B. Taylor, A.G. Dall'Asén, D.K. Roper, Electroless gold island thin films: photoluminescence and thermal transformation to nanoparticle ensembles, Langmuir 24(8) (2008) 4174-4184.

[40] M.L. Coluccio, F. Gentile, M. Francardi, G. Perozziello, N. Malara, P. Candeloro, E. Di Fabrizio, Electroless deposition and nanolithography can control the formation of materials at the nano-scale for plasmonic applications, Sensors 14(4) (2014) 6056-6083.

[41] Z. Wei, F.P. Zamborini, Directly monitoring the growth of gold nanoparticle seeds into gold nanorods, Langmuir 20(26) (2004) 11301-11304.

[42] K.M. Koczkur, S. Mourdikoudis, L. Polavarapu, S.E. Skrabalak, Polyvinylpyrrolidone (PVP) in nanoparticle synthesis, Dalton Transactions 44(41) (2015) 17883-17905.